

Multibody models with flexible components for inflatable space structures

Marco Petrolo*¹, Giorgio Governale^{1a}, Daniele Catelani^{2b} and Erasmo Carrera^{1c}

¹MUL² Group, Department of Mechanical and Aerospace Engineering, Politecnico di Torino, Corso Duca degli Abruzzi 24, 10129, Torino, Italy

²MSC Software srl, Via Santa Teresa 12, 10121 Torino, Italy

(Received January 19, 2018, Revised February 26, 2018, Accepted February 27, 2018)

Abstract. This work has the objective to analyze multibody mechanisms of inflatable structures for manned space applications. The focus is on the evaluation of the main characteristics of MaxFlex, a new module of MSC Adams including the effect of nonlinear flexible bodies. MaxFlex integrates the nonlinear Finite Element Analysis (FEA) of Nastran—SOL400—and the Adams multibody capabilities in one unique solver, providing an improvement concerning the concept and technology based on the co-simulation among solvers. MaxFlex converts the equations of motion of the nonlinear FEA into phase-space form and discretizes them according to the multibody system integrator framework. The numerical results deal with an inflatable manned space module having rigid components and a flexible coating made of Kevlar. This paper is a preliminary assessment of the computational capabilities of the software and does not provide realistic guidelines for the actual design of the structure. The analysis leads to some recommendations related to the main issues to consider in a nonlinear simulation including both rigid and flexible components. The results underline the importance of realistic deployment times and applied forces. Also, a proper structural modeling is necessary, but can lead to excessive computational overheads.

Keywords: multibody; MSC Adams MaxFlex; nonlinear; inflatable structures

1. Introduction

Gossamer structures—also known as Inflatable Structures (IS)—possess special properties such as low weight, minimal stowage volume, and high strength-to-mass ratio. Recently, IS have found increasing opportunities in many engineering applications (Cadogan and Grahne 1999, Greschik and Park 1996a, b, Seffen and Pellegrino 1999, Chmielewski *et al.* 2000). In spacecraft engineering, the possibility of inflating structures in orbit is of interest and typical applications for space systems are

- manned modules (Kennedy *et al.* 2000, Hinkle and Lin 2009),
- re-entry systems (Wilde *et al.* 2002), aerobraking and de-orbiting, (Santerre and Cerf 2009,

*Corresponding author, Professor, E-mail: marco.petrolo@polito.it

^a Research Assistant, E-mail: giorgio.governale@polito.it

^b Senior Project Manager, E-mail: daniele.catelani@mscsoftware.com

^c Professor, E-mail: erasmo.carrera@polito.it

Nock *et al.* 2010),

- solar sails (Seefeldt *et al.* 2017),
- antennas (Huang 2001),
- landing systems (Cadogan *et al.* 2002),
- sunshields (Ewing *et al.* 2009).

An important characteristic of IS is the possibility to exploit a habitable volume greater than traditional metallic space modules assuring, among other things, the possibility of increasing the comfort and the number of crew members on board with a consequent benefit for the entire mission result (Nebiolo *et al.* 2015). The present paper focuses on IS for manned modules. An early example of manned inflatable space modules is the NASA TransHab (Kennedy and TX 2002), an inflatable module with a central structural core conceived as a habitation module for the International Space Station (ISS). The latest example of gossamer structures for manned modulus is the Bigelow Expandable Activity Module (Valle and Wells 2017) recently berthed to the ISS.

Most of the design and verification of IS requires experimental activities. In fact, the simulation of IS via computational mechanics is not an easy task. The analysis involves strong nonlinearities, membrane materials, multibody motions, and large deformations. There is an increasing interest in the development of computational mechanics tools for IS to augment the reliability of virtual experiments. Examples of recent developments have focused on the investigation on the structural nonlinearities (Jhaa and Inman 2004, Elsabbagh 2015), nonlinear structural analyses via beam finite elements (Thomas and Bloch 2016), impact analysis (Graczykowski 2016, Kim *et al.* 2017), stability analysis (Roychowdhury and DasGupta 2015), fluid-structure interactions (van Opstal *et al.* 2015), assessment of finite elements (Lampani and Gaudenzi 2010), aerothermodynamics (Guo *et al.* 2017), modal analysis (Hu *et al.* 2017) and deployment simulation (Sosa *et al.* 2016).

This paper presents numerical investigations on the behaviour of IS that exhibit strong nonlinearities via the multibody method. The analysis made use of a new module of MSC Adams, MaxFlex (Adams MaxFlex 2016). MaxFlex can simulate complex multibody systems by integrating flexible bodies with nonlinear behavior. MaxFlex combines the finite element solver of MSC Nastran with the multibody model analysis of Adams with no need of co-simulations between two different software (Collingridge *et al.* 2014a). This paper is organized as follows: Section 2 describes the main features of the model, Section 3 presents the numerical results and their discussions, and Section 4 presents the main conclusions of this work.

2. Flexible multibody theory

The Euler-Lagrange equation for a multibody system is

$$\frac{d}{dt} \left(\frac{\partial \mathbf{L}}{\partial \dot{\mathbf{q}}} \right) - \frac{\partial \mathbf{L}}{\partial \mathbf{q}} + \boldsymbol{\Phi}_q^T \boldsymbol{\lambda} = \mathbf{Q} \quad (1)$$

where \mathbf{L} is the Lagrangian equation of the system, given by the difference between kinetic and potential equation of a rigid body, \mathbf{q} is the vector of generalized coordinates, while $\boldsymbol{\lambda}$ contains Lagrange multipliers, referred to as binding reactions. Constraint equations are contained in $\boldsymbol{\Phi}$ and the parameter

$$\boldsymbol{\Phi}_q = \frac{\partial \boldsymbol{\Phi}}{\partial \mathbf{q}} \quad (2)$$

represents the Jacobian matrix of constraints. \mathbf{Q} is a vector representing the external applied forces, balanced by the acceleration, the potential force and Lagrange multipliers. The *ADAMS/Solver* implements the following set of equations (Collingridge *et al.* 2014b),

$$M\ddot{\mathbf{q}} + \dot{M}\dot{\mathbf{q}} - \frac{1}{2}\dot{\mathbf{q}}^T \frac{\partial M}{\partial \mathbf{q}} \dot{\mathbf{q}} + \frac{\partial V}{\partial \mathbf{q}} + \Phi_q^T \lambda = \mathbf{Q} \quad (3)$$

Considering n differential second-order equations and m constraint equations in which

- n is the number of bodies;
- M is the mass matrix $n \times n$;
- $\frac{1}{2}\dot{\mathbf{q}}^T \frac{\partial M}{\partial \mathbf{q}} \dot{\mathbf{q}}$ is total kinetic energy;
- V is the system potential energy;
- Φ_q is the Jacobian constraint matrix $m \times n$;
- \mathbf{Q} is the column vector $n \times 1$ representing the applied forces.

The *Adams* explicit integrator ABAM (Adams Bashforth-Adams Moulton) uses a prediction-validation-correction-validation system to integrate a set of Ordinary Differential Equations (ODE), reducing the whole system of differential algebraic equations to a set of ordinary differential equations. This method selects and integrates only the Degree of Freedoms (DOF) that change most during the simulation (Negrut and Dyer 2004).

Traditional flexible MultiBody Dynamics (MBD) model parts using flexible bodies are based on linear deformations. *ADAMS MaxFlex* adopts nonlinearities in the finite element components of the analysis via the generalised α -method (Negrut *et al.* 2006) to solve a system of linearized equations such as:

$$M\ddot{u} + B\dot{u} + Ku = R \quad (4)$$

where M , B and K are the mass, damping and stiffness matrices, respectively, and R is the residual vector (Negrut *et al.* 2006). The displacements vector u includes both translational and rotational components. Using a time integrator,

$$\left[\frac{M}{\beta h^2} + \frac{B}{\beta h} + K \right] \delta u = R \quad (5)$$

where β is an integration parameter and h the time step. This equation is valid only for a normal transitory step, where the time step h is not zero, therefore, cannot be applied to initial and redundant conditions, nor to static equilibrium analysis, which requires a special treatment. To couple the FE equations with the multibody ones, the phase-space form is used,

$$Ax = \begin{bmatrix} \frac{M}{\beta h} + B & K \\ -I & \frac{I}{\beta h} \end{bmatrix} \begin{Bmatrix} v \\ u \end{Bmatrix} = \begin{Bmatrix} R \\ \dot{u} - v \end{Bmatrix} \quad (6)$$

A flexible *nonlinear* body is modelled as an external component to the multibody code; the coupling between MBS and FE equation is carried out via the markers on the interface grids, defined in both domains, and by constraint equations defined to improve kinematic compatibility between states.

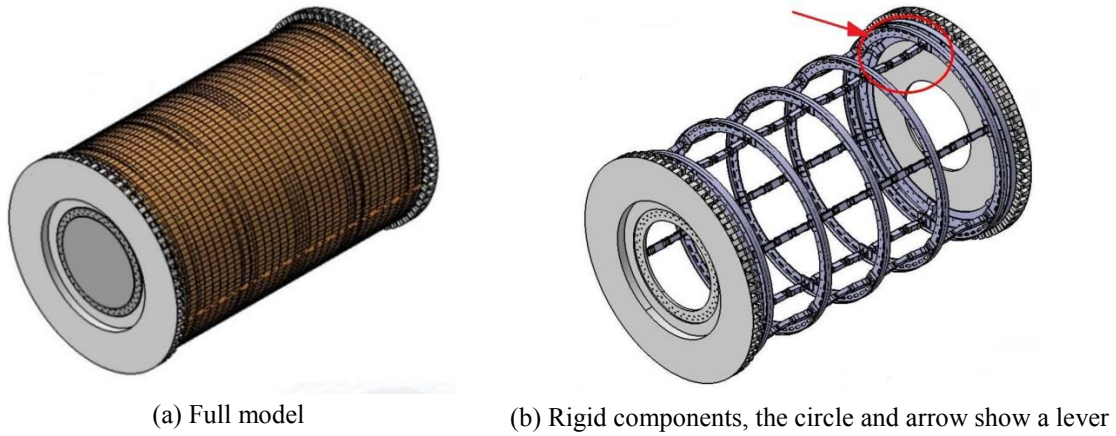


Fig. 1 Inflatible manned structure (Nebiolò *et al.* 2015)

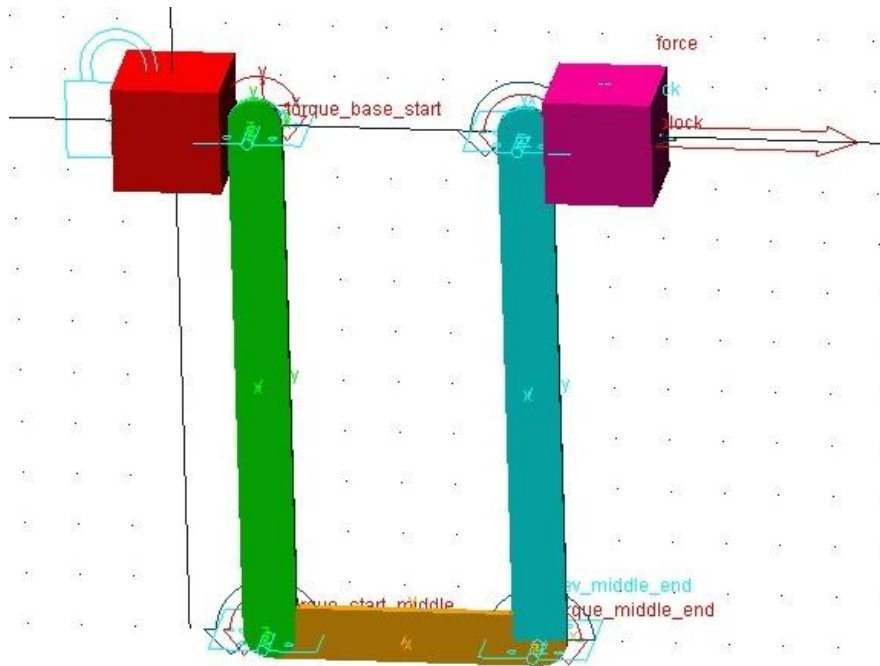


Fig. 2 Model 1, lever mechanism

Table 1 Model 1 geometry

Body part	Length [mm]	Width [mm]	Depth [mm]
Starting Block	50	50	50
Lever 1	272	50	60
Lever 2	190	40	60
Lever 3	272	50	60
End block	50	50	50

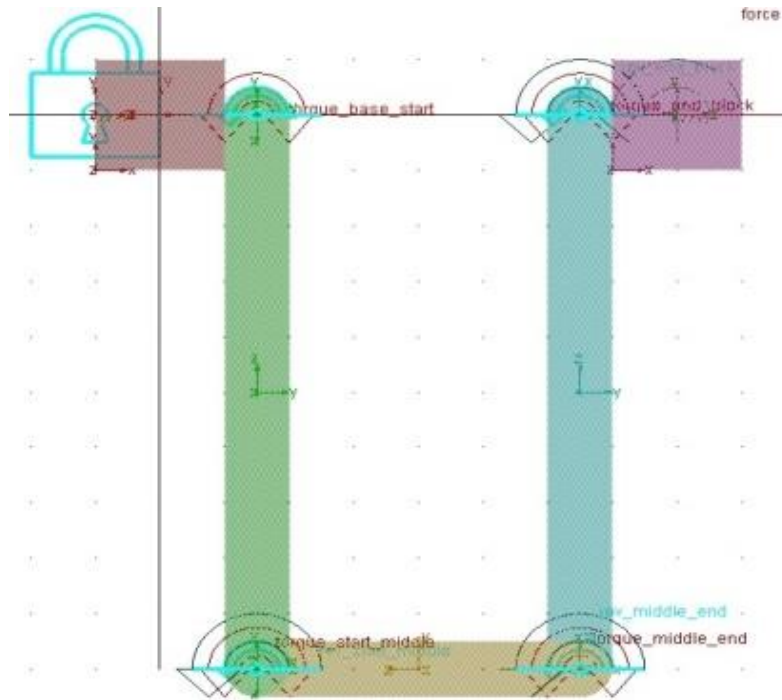


Fig. 3 Model 1, joint connectors

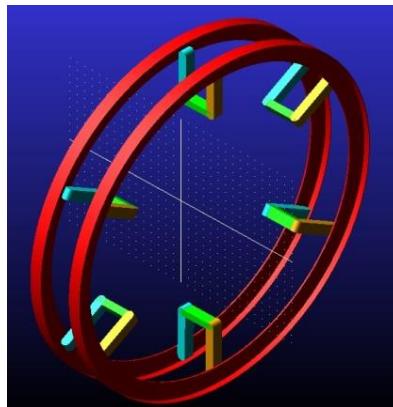


Fig. 4 Model 2, ribs and levers

3. Model evolution

This section describes the models analysed in this paper. Increasingly complexity was achieved by adding additional features to subsequent models.

Figure 1 shows the IS considered in this paper. The main cylindrical structure has a coating made of Kevlar strips in the longitudinal and circumferential directions, in particular, 62 longitudinal strips. The red circle in Fig. 1 (b) shows the section of the mechanism considered in this paper, see Fig. 2. Model 1 is used to test and develop a proper joint configuration. The geometrical characteristic are reported in Table 1.

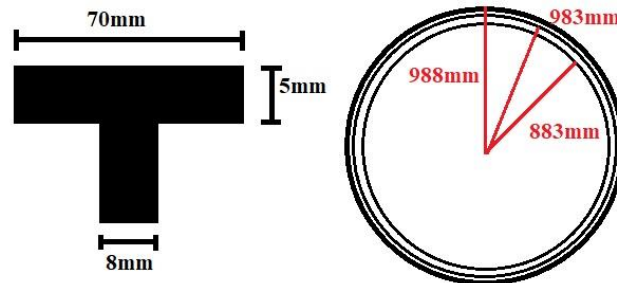


Fig. 5 Rib geometry

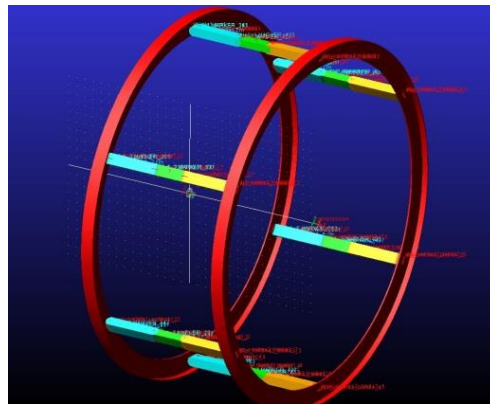


Fig. 6 Model 3, closing model

Figure 3 shows the joints used in model 1. The starting block is connected to the ground through a fixed joint, while a revolute joint is used to connect the remaining bodies. The revolute joints have torsion forces limiting their rotations. The angle between two levers cannot be lower than 90° . Such forces stem from the application of a BISTOP function, which is a built-in function representing a two-side impact force. The BISTOP will prevent unwanted behaviours and keep the mechanism locked once open. Both blocks and levers are realised with standard aluminium, whose properties are pre-set into the software. The traction force applied to the end block is defined by a STEP function with starting values of 0 s and 0 N and end values of 1 s and 100 N. Model 2 has ribs, as shown in Fig. 4. The lever dimensions are the same as model 1, while the ribs have a T section, see Fig. 5. Aluminium is the material of all rigid components, as it is pre-set in the software. The distance between the centre of mass (CM) of the two ribs is 260 mm.

The revolute joints between levers and ribs are replaced with flexible connections via bushing forces. The design variables used to define the bushing forces have the following values:

- $K_{tra} = 1e4 \text{ N/mm}$
- $C_{tra} = 10 \text{ Ns/mm}$
- $K_{rot} = 1e6 \text{ Nmm/}^\circ$
- $C_{rot} = 1000 \text{ Nmms/}^\circ$
- $K_{rotz} = 80 \text{ Nmm/}^\circ$
- $C_{rotz} = 50 \text{ Nmms/}^\circ$

where K_{tra} and C_{tra} are the translational stiffness and damping, respectively, and set in all 3

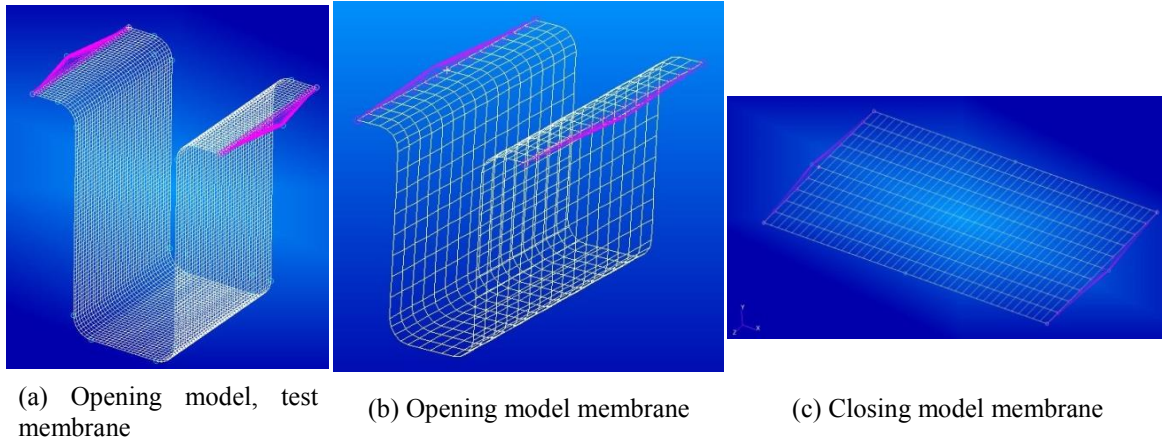


Fig. 7 FE membranes

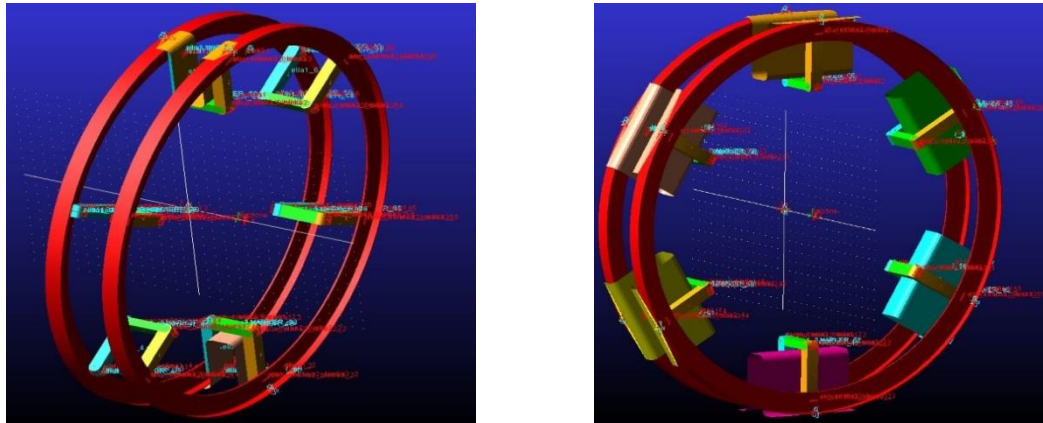
directions of the bushings. K_{rot} and C_{rot} are rotational stiffness and damping, set in the X and Y direction, while K_{rotz} and C_{rotz} are the rotational stiffness and damping in the Z direction. A low value of stiffness and damping in the Z rotational component allows the system to move fluidly. Having replaced the revolute joint with bushing forces, the STEP function of the joint motion has to take into account the blocking of the system at the end position. The applied force on the right rib is defined by a STEP function with starting values of 0 s and 0 N and end values of 5 s and 30000 N.

Model 3 was used to simulate the closing mechanism. In model 3, ribs are 804 mm distant, see Fig. 6. An imperfection of 0.1° was introduced while rotating the levers to prevent the system from having a perfectly horizontal set of levers, which would introduce a singularity in the calculations. The locking mechanism ensured by the BISTOP inside the step function activates once the system is in closed position. The closing force is a linear function from 0 N at 0 s to 500 N at 1 s.

Model 4 has two flexible membranes on the rigid body from model 2. Due to the limited computational capacity, a circular membrane is not feasible, therefore, an approximated model is chosen, with a series of strips imported as independent flexible bodies. The flexible strips have membranal Young modulus of 87000 MPa, while the bending one is 870 MPa. In both cases, the Poisson ratio is 0.34 and the density 1370 Kg/m³, while thickness is 0.3 mm. Rigid body elements—RBE2—connect the flexible strips to the ribs. Due to the inherent stiffness of the membrane, a new applied force was used. The force law has a starting value of 0 N at 0 s, reaches 1000 N in 5 s with a linear function, and continues to 26000 N in further 10 s.

The opening model membrane follows the initial configuration of the levers, having a U shape with a total length of 804 mm. The width chosen for the initial tests was 200 mm, see Fig. 7 (a) and 8 (a). Once model 4 proved functional, model 5 with a width of 465 mm has been created, with six flexible bodies instead of two, see Fig. 7 (b). This width was determined considering the real model, constituted of 62 strips, and dividing their total width by 6. The applied force necessary to open the mechanism with six flexible bodies uses two successive STEP functions. The first one from 0 N at 0 s to 250 N in at 5 s, the second one from 250 N at 5 s to 20000 N at 20 s. The closing membrane shown in Fig. 7 (c) has the same characteristics of the previous ones, but a flat shape, and is used for model 6.

Model 4 is reported in Fig. 8 (a), while the complete opening mechanism, model 5, is shown in



(a) Model 4, two membranes

(b) Model 5, six membranes

Fig. 8 Multibody models with two and six flexible components

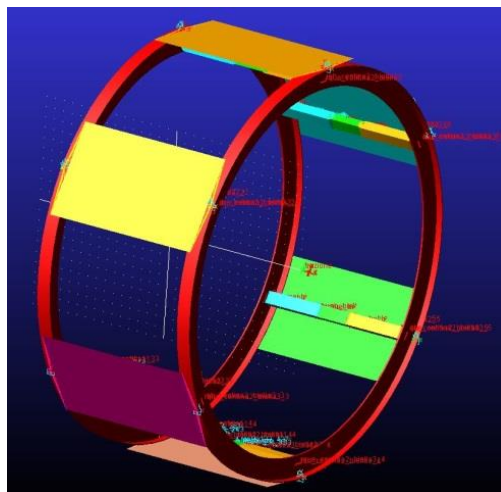
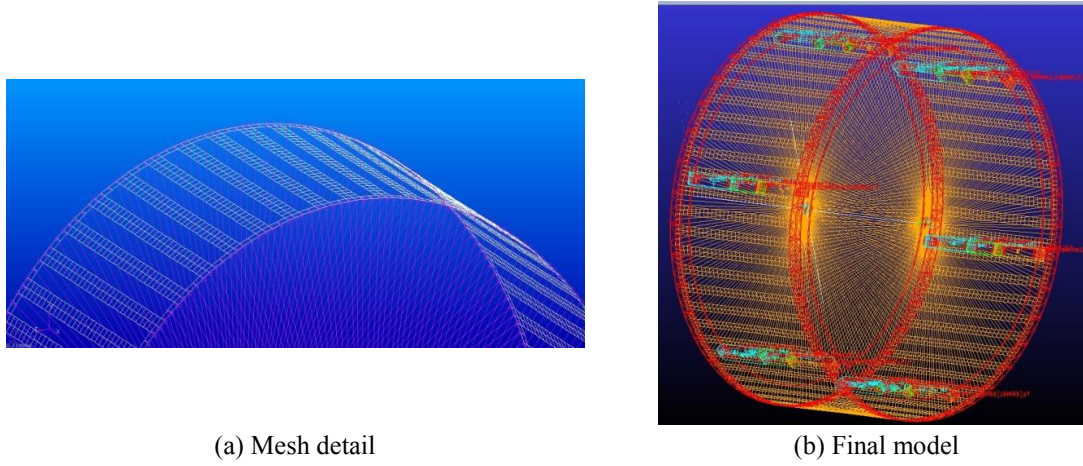


Fig. 9 Model 6, closing mechanism with six membranes

Fig. 8 (b). Once the total deployment of the structure has been obtained, the closing mechanism was considered, see Fig. 9. The closing force uses a STEP function going from 0 N at 0 s to 500 N at 5 s.

In model 7, instead of importing different flexible bodies, a geometry with a single structural component was considered, see Fig. 10 (a). The 62 longitudinal strips seen in Fig. 1 (a) are connected via a circumferential strip at each end, to avoid geometrical discontinuities. Instead of different flexible components, there is only one flexible membrane which covers the entire rigid body, see Fig. 10 (b). The applied force is shown in Fig. 11, and has a constant value of 600 N from 0 s to 3 s, then decreases to 500 N with a STEP function ending at 5 s, and goes to 700 N via a second STEP function ending at 8 s. The complex definition of the force follows the different requirements of the mechanism during the analysis. An initial value of force sets the system in motion, but causes an extreme acceleration that could bring the simulation to failure. Reducing the magnitude of the force granted a smoother simulation, allowing the calculation to proceed. Once



(a) Mesh detail (b) Final model

Fig. 10 Complete flexible membrane, applied on Model 3

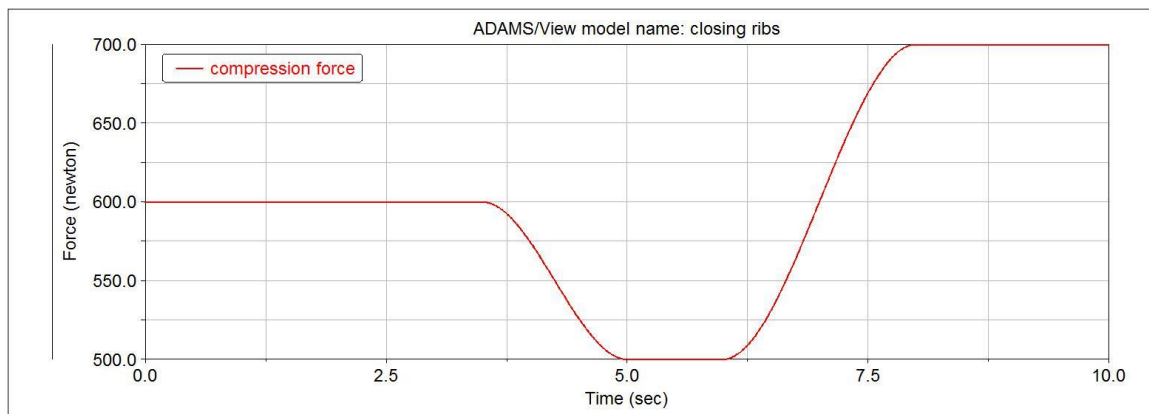


Fig. 11 Model 7 applied force

Table 2 Models and their main components

Model number	Model Type	Rigid bodies	Number of flexible membranes	Type of flexible membranes
1	Opening	Levers	0	N/A
2	Opening	Levers, ribs	0	N/A
3	Closing	Levers, ribs	0	N/A
4	Opening	Levers, ribs	2	Independent strips
5	Opening	Levers, ribs	6	Independent strips
6	Closing	Levers, ribs	6	Independent strips
7	Closing	Levers, ribs	62	Strips connected via two rings

the membrane starts to deform, an inner stiffness starts to arise, interfering with the closing mechanism, making it necessary to raise the force to a higher value, to reach the complete closing. Table 2 contains a summary of the different models realized and their main characteristics.

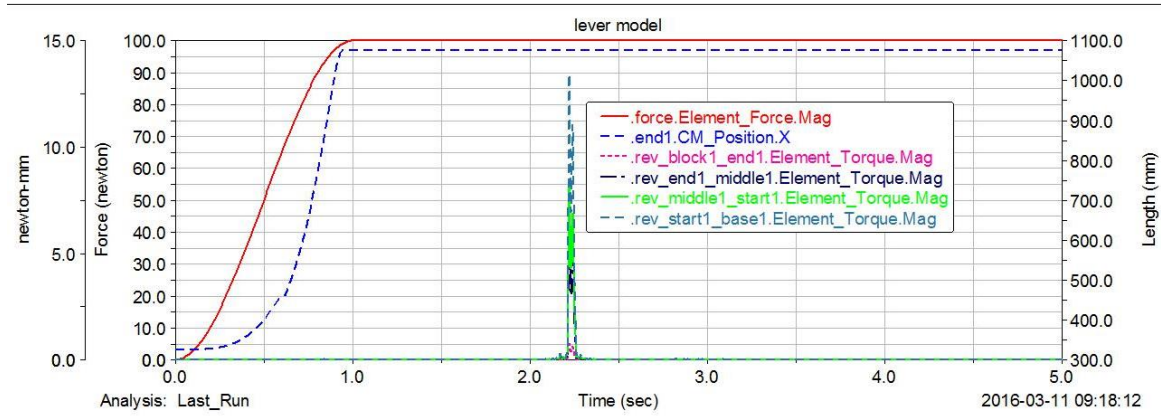


Fig. 12 Force history and center of mass position in the case of two flexible components

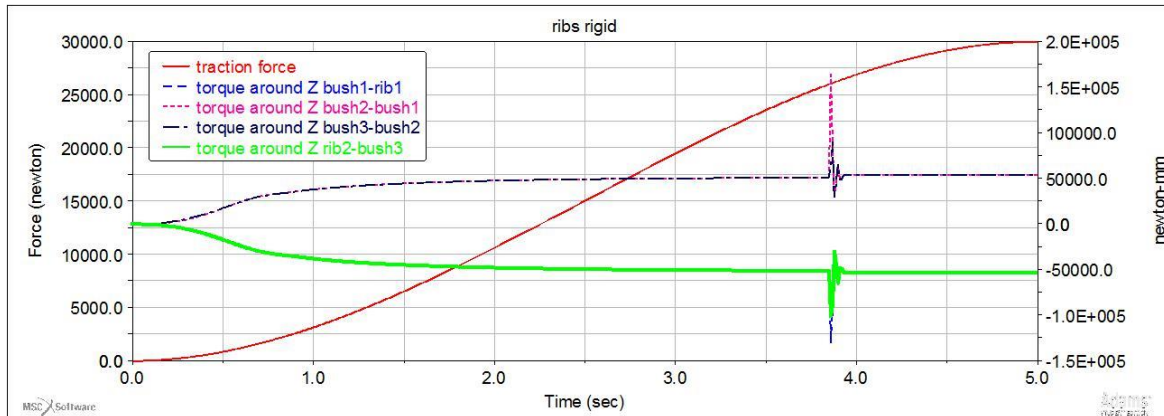


Fig. 13 Force history and bushing torque reaction on model 2

4. Results

The results are divided into two main groups, model 1 to 3 contain only rigid body, while model 4 to 7 have also flexible components.

4.1 Rigid multibody models

The aim of this analysis is the definition of the force to apply to simulate the deployment of the system. In fact, the applied forces must allow the complete deployment in a limited amount of time and avoid excessive accelerations. Model 1 force results are reported in Fig. 12. This model has been realized as a test to assess the functionality of the mechanism before proceeding to the actual case study.

The guidelines stemming from this case are the following:

- STEP functions can be used to block the model in an open position.
- Revolute joints need a second STEP function to prevent unwanted behavior in the opening phase.

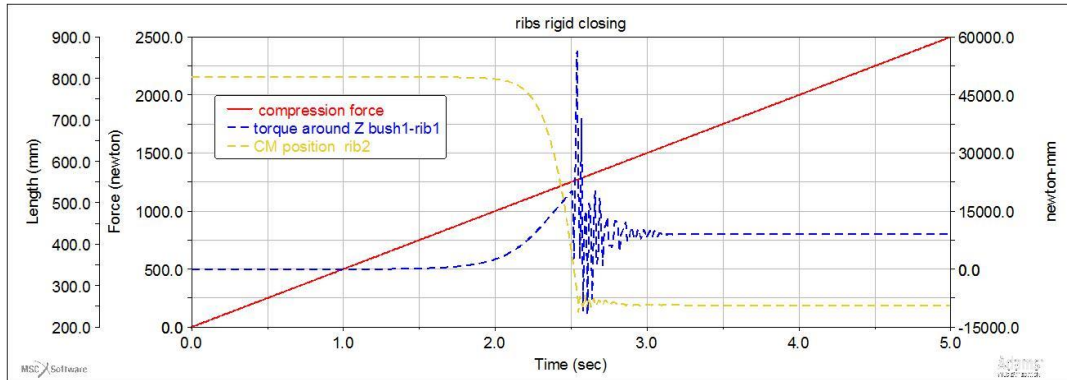


Fig. 14 Force history, center of mass position and torque reaction on one bushing for model 3

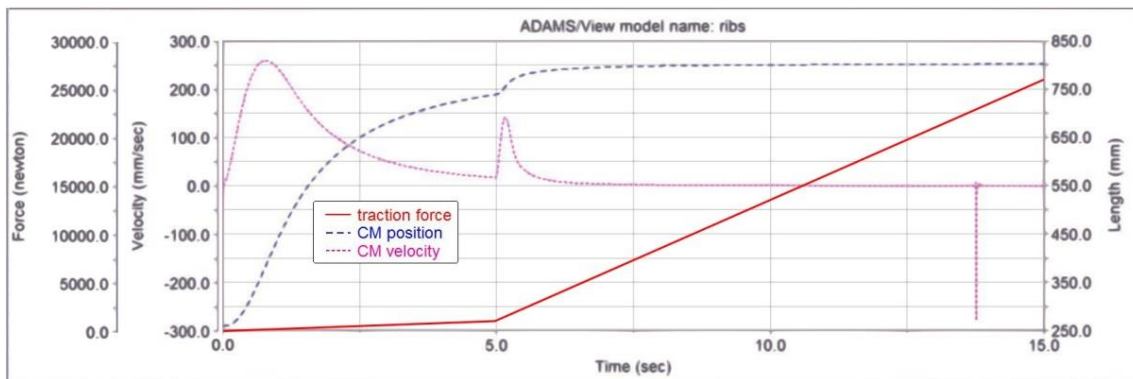


Fig. 15 Force, centre of mass position and velocity in model 4

- The complete opening of the mechanism is visible in the graphic after less than 1 s, but the locking mechanism will activate at around 2 s, thanks to the peaks of torque reactions.

Model 2 results are depicted in Fig. 13 in which the rigid opening model used to test the force laws necessary to allow the later application of the flexible membranes. The complete opening of the rigid mechanism is obtained in less than 5 seconds.

This case suggests that

- The definition of the force with a step function avoids excessive accelerations.
- A flexible joint such as the bushing introduces a rotational stiffness, requiring a higher force to initialize motion.
- The use of bushing forces allows to remove the second STEP function defined in every joint.
- The resulting torque reaction shown in Fig.13 is proportional to the design values used for stiffness and damping.

Model 3 results are shown in Fig. 14. To determine the value of force necessary to close the mechanism, the position of the left rib CM must be evaluated.

The following conclusions can be obtained from this case:

- A low magnitude of force is enough for motion, and the use of a linear function is effective. The inherent stiffness of a bushing joint is not enough to allow a smooth closing, and the mechanism reaches the closed configuration in a short amount of time.

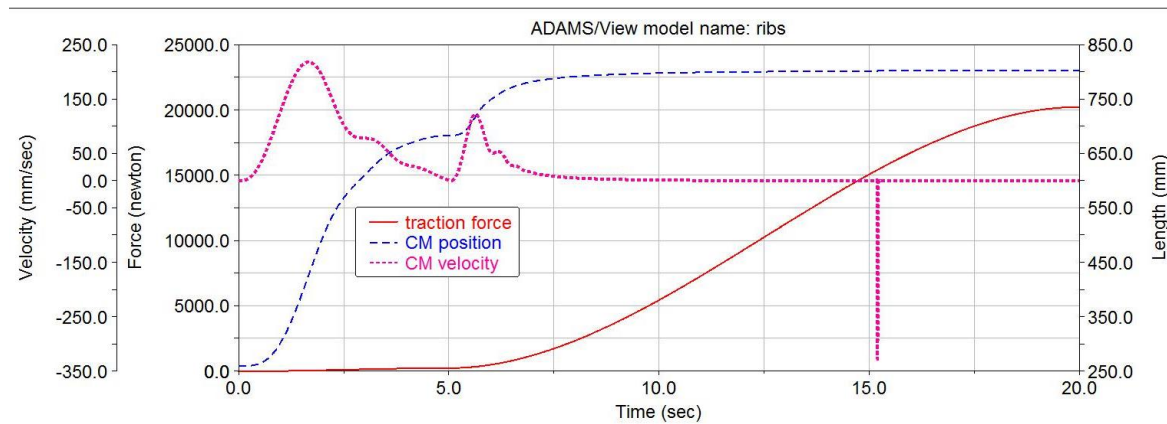


Fig. 16 Force, centre of mass position and velocity in model 5

- The CM starts moving at 2 s with a force of 1000 N and reaches the complete lock of the mechanism at 2.5 s, with an acceleration that could be critical once flexible bodies are added.

Every test performed on the rigid body model has taken in account a time of 5 s, while the realistic time should be of hours, to reduce the computational cost. To perform analysis with flexible bodies, this time has been extended, to avoid rapid deformations.

4.2 Rigid models with flexible membranes

Model 4 represents the first step in the analysis of a rigid structure with flexible membranes. Two membranes are used to guarantee the symmetry of the system. Results obtained for this model are depicted in Fig. 15. The main conclusions from the analysis of the force history are the following:

- A double slope is advisable. In fact, the imposition of a strong initial impulsive force can cause numerical instabilities due to the excessive deformations in the flexible components.
- In the initial deployment phase, the velocity increases and then decreases. In fact, after the initial deployment, the stiffness of the flexible components tends to decrease the system speed.
- Around 5 s, the opening velocity is almost zero. A change of the force slope allows to complete the simulation.
- The velocity graph shows how the system reaches a constant value in a short amount of time, avoiding undesired accelerations.
- The peak in the velocity plot at 14 s is due to the activation of the locking mechanism or bistop. The activation of such mechanism leads to abrupt accelerations and smaller time steps, therefore, higher computational costs.

Model 5 is the evolution of the previous case. Due to the presence of more flexible bodies, the system will be more sensible to excessive accelerations. To compensate the addition of more flexible bodies to the system, the rotational stiffness of the bushing is strongly reduced, to allow to obtain a complete opening even with lower forces. Figure 16 shows the results obtained in this case.

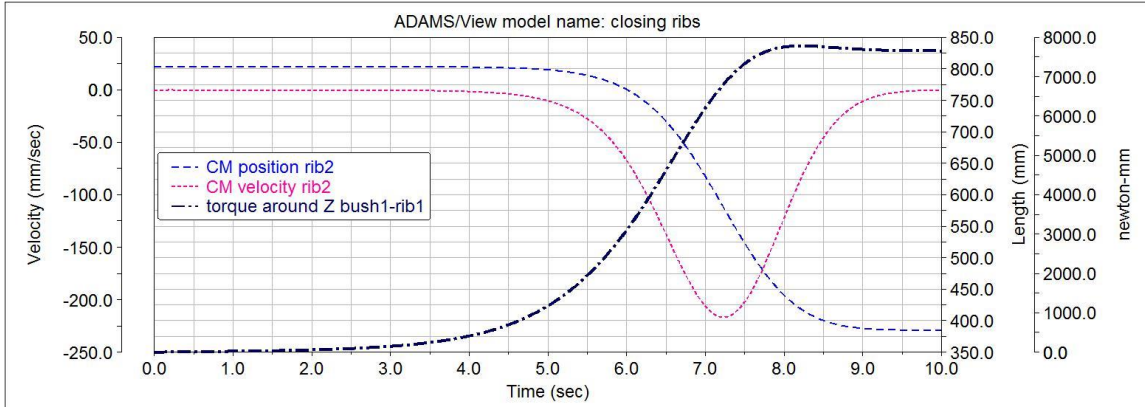


Fig. 17 Force, centre of mass position and velocity in model 6

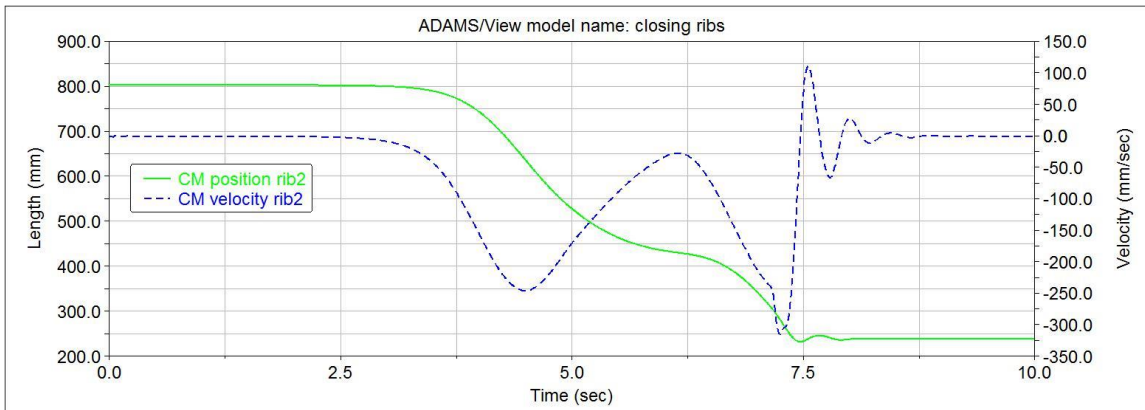


Fig. 18 Centre of mass position and velocity in model 7

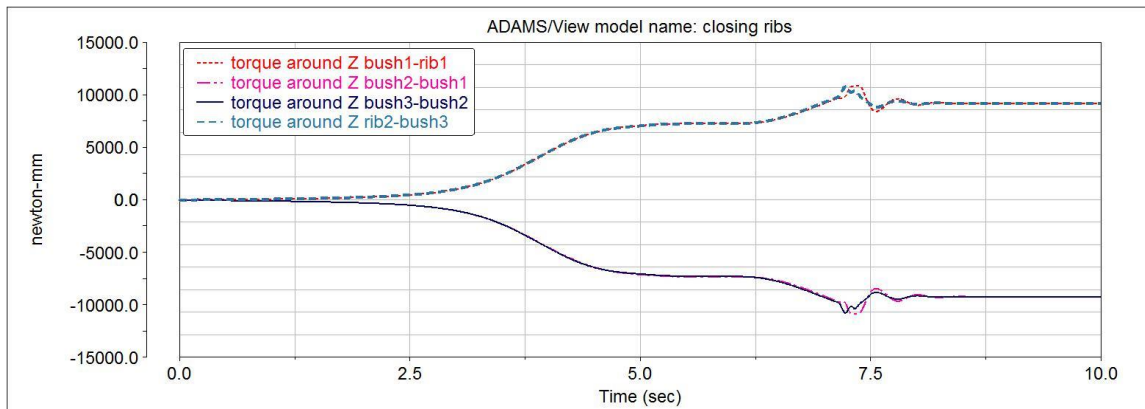


Fig. 19 Torque reaction on bushings in model 7

The main results of this case are the following:

- The force function has been modified with two consecutive STEP leading to a maximum velocity lower than the previous case.
- The inner stiffness of the membranes causes the velocity to have a less smooth transition to

a zero value.

- A longer amount of time is required for this simulation to obtain a complete locking of the system.

Model 6 is a closing model with six independent flexible bodies, making its computational burden quite high. Figure 17 shows the results obtained for this simulation. The main results of this case are the following:

- Being a closing model, the force function is modelled to not induce too large accelerations on the system, as shown in the previous section.
- As visible from the torque graphic, a complete closing has not been reached due to the type of force applied.

Model 7 is more realistic than 6 and results are depicted in Fig. 18 and Fig. 19. The model contains a single flexible body, shaped to better reproduce the real configuration. The model 7 results suggest that

- The double STEP force function depicted in Fig. 11 allows the system to smoothly reach the closed configuration.
- Compared to the previous case, a time of 10 seconds is more than enough to close and lock the system, Fig. 17 shows how the velocity has already reached a zero value at 8 s.
- The opportune definition of the design variables of the bushing allows to have a soft reaction on the system, as visible thanks to the peaks in torque in Fig. 18, preventing excessive accelerations.
- Considering the time required to perform the analysis, model 7 has proved to be much more efficient than the previous one, going from the 8 hours required for model 6 to merely 2 hours.

Every analysis has considered a deployment time of 10 to 20 s, although a realistic one should be of hours. Such a choice allows shorter analyses and does not compromise the aims of the work. This study must be considered as a preliminary assessment of the computational capabilities of the software and does not provide realistic guidelines for the actual design of the structure.

5. Conclusions

The aim of this paper is the evaluation of MaxFlex, a new module of MSC Adams including the effect of nonlinear flexible bodies in the multibody analysis. MaxFlex integrates the nonlinear finite element analysis (FEA) of Nastran—SOL400—and the Adams multibody capabilities in one unique solver, providing an improvement concerning the concept and technology based on the co-simulation among solvers. Assessments have focused on the nonlinear analysis of an inflatable manned space module to investigate the limits and the most useful features of the software, and to provide guidelines on the multibody analysis including nonlinear finite elements.

The main outcomes are the following:

- The flexible bodies can undergo excessive accelerations and deformations with consequent numerical instabilities and loss of accuracy.
- The definition of the forces acting on the system is a nontrivial task. A more detailed analysis of forces is advisable to avoid numerical instabilities and/or failure of the simulation.
- The implementation of flexible bodies on the rigid structures requires a modification of the applied forces to consider the increased stiffness of the global system.

- The intermediate and final stages of the simulation are particularly critical. In the former, the velocity of the flexible components may be excessive. In the latter, the introduction of bistops to impose the closing may lead to peaks in the acceleration and increment in the computational times.
- The study of an opening mechanism has proved different from the closing one regarding the determination of the force function law. The former will require a double step function with increasing value, and high total magnitude of force. The latter needs low forces, and a decreasing step followed by an increasing one to avoid excessive accelerations.
- The reduction of the number of flexible bodies, together with the increase of their geometrical accuracy, has proved to reduce the computational costs.
- A decrease in the rotational stiffness of the bushing constraint can reduce the magnitude of force required to perform the simulation. Flexible bodies should always be realized with simple geometries, avoiding edges which could bring to numerical instabilities or simulation failure.

Future works should consider the refinement of the finite element model of the flexible component to evaluate stress distributions. In fact, this work adopted coarse meshes and 2D elements to limit the computational costs. However, such a choice can lead to unreliable results for this type of structural components. The geometry considered for the flexible membrane represents only the longitudinal stripes of the real structure, a more detailed model could be realized implementing the circumferential stripes. A further future work could consist in the validation of the computational framework through a simple test experience, allowing to quantify the correlation reached.

References

- Adams MaxFlex (2016), Adams MaxFlex Theory, MSC Software Corporation; CA, U.S.A.
- Cadogan, D.P. and Grahne, M.S. (1999), "Deployment control mechanism for inflatable space structures", *33rd Aerospace Mechanism Conference*, Pasadena, U.S.A., May.
- Cadogan, D., Sandy, C. and Grahne, M. (2002), "Development and evaluation of the Mars pathfinder inflatable airbag landing system", *Acta Astronautica*, **50**(10), 633-640.
- Chmielewski, A.B., Moore, C. and Howard, R. (2000), "The gossamer initiative", *Proceedings of 2000 IEEE Aerospace Conference*, MT, U.S.A., March.
- Collingridge, M., Patel, H., Riley, S. and Shen, W. (2014a), "Multibody dynamics integration of nonlinear finite element components", *NAFEMS Americas Conference*, Colorado Springs, U.S.A., May.
- Collingridge, M., Riley, S., Shen, W. and Patel, H. (2014b), "Coupling of a nonlinear finite element solver in multibody dynamics", *3rd Joint International Conference on Multibody System Dynamics and 7th Asian Conference on Multibody Dynamics*, Busan, Korea, June.
- Elsabbagh, A. (2015), "Nonlinear finite element model for the analysis of axisymmetric inflatable beams", *Thin Wall. Struct.*, **96**, 307-313.
- Ewing, A.P., Back, J.M., Schuettelz, B.M. and Laue, G.P. (2009), "James Webb space telescope sunshield membrane assembly", *50th AIAA/ASME/ASCE/AHS/ASC Structures, Structural Dynamics, and Materials Conference*, Palm Springs, U.S.A., May.
- Graczykowski, C. (2016), "Mathematical models and numerical methods for the simulation of adaptive inflatable structures for impact absorption", *Comput. Struct.*, **174**, 3-20.
- Greschik, G. and Park, K.C. (1996a), "Helically curved unfurlable structural elements: kinematic analysis and laboratory demonstration", *J. Mech. Design*, **118**(1), 22-28.
- Greschik, G. and Park, K.C. (1996b), "The deployment of curved closed tubes", *J. Mech. Design*, **118**(3),

- 337-339.
- Guo, J., Lina, G., Bua, X., Fub, S. and Chaob, Y. (2017), "Effect of static shape deformation on aerodynamics and aerothermodynamics of hypersonic inflatable aerodynamic decelerator", *Acta Astronautica*, **136**, 421-433.
- Hinkle, J. and Lin, J.K.H. (2009), "Deployment testing of an expandable lunar habitat", *AIAA SPACE 2009 Conference and Exposition*, Pasadena, U.S.A., September.
- Hu, Y., Chen, W., Chen, Y., Zhang, D. and Qiu, Z. (2017), "Modal behaviors and influencing factors analysis of inflated membrane structures", *Eng. Struct.*, **132**, 413-427.
- Huang, J. (2001), "The development of inflatable array antennas", *IEEE Antennas and Propagation Magazine*, **43**(4), 44-50.
- Jhaa, A.K. and Inman, D.J. (2004), "Importance of geometric non-linearity and follower pressure load in the dynamic analysis of a gossamer structure", *J. Sound Vib.*, **278**(1-2), 207-231.
- Kennedy, K.J., Raboin, J., Spexarth, G. and Valle, G. (2000), "Inflatable structures technology handbook: Chapter 21 inflatable habitats", JSC-CN-6300; NASA Johnson Space Center; Houston, TX, U.S.A.
- Kennedy, K.J. and TX, R.A. (2002), "Lessons from TransHab: An architect's experience", *AIAA Space Architecture Symposium*, Houston, U.S.A., October.
- Kim, Y., Choi, C., Sarath Kumar, S.K.S. and Kim, C.G. (2017), "Hypervelocity impact on flexible curable composites and pure fabric layer bumpers for inflatable space structures", *Composite Structures*, **176**, 1061-1072.
- Lampani, L. and Gaudenzi, P. (2010), "Numerical simulation of the behavior of inflatable structures for space", *Acta Astronautica*, **67**(3-4), 362-368.
- Nebiolo, M., Simone, A., Messidoro, A., Ferraris, M., Carrera, E., Maggiore, P. and Valletti, D. (2015), "New inflatable habitats generation", *23rd Conference of the Italian Association of Aeronautics and Astronautics*, Torino, Italy, November.
- Negrut, D. and Dyer, A. (2004), *ADAMS/Solver Primer*, MSC Software Documentation, Ann Arbor, U.S.A.
- Negrut, D., Rampalli, R., Ottarsson, G. and Sajdak, T. (2006), "On an implementation of the Hilber-Hughes-Taylor method in the context of index 3 differential-algebraic equations of multibody dynamics", *J. Comput. Nonlinear Dyn.*, **2**(1), 73-85.
- Nock, K.T., Gates, K.L., Kim, A.M. and McRonald, A.D. (2010), "Gossamer Orbit Lowering Device (GOLD) for safe and efficient de-orbit", *AIAA/AAS Astrodynamics Specialist Conference*, Toronto, Canada, August.
- Roychowdhury, S. and DasGupta, A. (2015), "On the response and stability of an inflated toroidal membrane under radial loading", *J. Non-Linear Mech.*, **77**, 254-264.
- Santerre, B. and Cerf, M. (2009), "The aerobraking sail for launcher upper stage deorbiting: concept feasibility and technological solutions", *5th European Conference on Space Debris*, Darmstadt, Germany, March.
- Seefeldt, P., Spietz, P., Sproewitz, T., Grundmann, J.T., Hillebrandt, M., Hobbie, C., Ruffer, M., Straubel, M., Toth, N. and Zander, M. (2017), "Gossamer-1: Mission concept and technology for a controlled deployment of gossamer spacecraft", *Adv. Space Res.*, **59**, 434-456.
- Seffen, K.A. and Pellegrino, S. (1999), "Deployment dynamics of tape springs", *Proceedings of the Royal Society of London Series A: Mathematical Physical and Engineering Sciences*, **455**, , 1003-1048.
- Sosa, E.M., Wong, J.C., Adumitroaie, A., Barbero, E.J. and Thompson, G.J. (2016), "Finite element simulation of deployment of large-scale confined inflatable structures", *Thin-Walled Struct.*, **104**, 152-167.
- Thomas, J.C. and Bloch, A. (2016), "Non linear behaviour of an inflatable beam and limit states", *Procedia Engineering*, **155**, 398-406.
- Valle, G. and Wells, N. (2017), "Bigelow Expandable Activity Module (BEAM) ISS Year-One", *ISS R&D Conference*, Washington, USA, July.
- van Opstala, T.M., van Brummelen, E.H. and van Zwieten, G.J. (2015), "A finite-element/boundary-element method for three-dimensional, large-displacement fluid-structure-interaction", *Computer Methods in Applied Mechanics and Engineering*, **284**, 637-663.

Wilde, D., Walther, S., Pitchadze, K., Alexsashkin, S., Vennemann, D. and Marraffa, L. (2002), "Flight test and ISS application of the Inflatable Reentry and Descent Technology (IRDT)", *Acta Astronautica*, **51**(1), 83-88.

AP